Applied Physics A (2021) 127:237
https://doi.org/10.1007/s00339-021-04366-3

Applied Physics A
Materials Science & Processing

Upgrading of methylammonium lead halide perovskite layers by thermal imprint

Andre Mayer[1] · Neda Pourdavoud[2] · Zineb Doukkali[1] · Kai Brinkmann[2] · Johannes Rond[1] · Johannes Staabs[1] · Ann-Christin Swertz[3] · Frederic van gen Hassend[4] · Patrick Görrn[1] · Thomas Riedl[2] · Hella-Christin Scheer[5]

Received: 5 August 2020 / Accepted: 12 February 2021 / Published online: 10 March 2021

Abstract
The manufacturing of devices from methylammonium-based perovskites asks for reliable and scalable processing. As solvent engineering is not the option of choice to obtain homogeneous layers on large areas, our idea is to 'upgrade' a non-perfect pristine layer by recrystallization in a thermal imprint step (called 'planar hot pressing') and thus to reduce the demands on the layer formation itself. Recently, imprint has proven both its capability to improve the crystal size of perovskite layers and its usability for large area manufacturing. We start with methylammonium lead bromide layers obtained from a conventional solution-based process. Acetate is used as a competitive lead source; even under perfect conditions the resulting perovskite layer then will contain side-products due to layer formation besides the desired perovskite. Based on the physical properties of the materials involved we discuss the impact of the temperature on the status of the layer both during soft-bake and during thermal imprint. By using a special imprint technique called 'hot loading' we are able to visualize the upgrade of the layer with time, namely a growth of the grains and an accumulation of the side-products at the grain boundaries. By means of a subsequent vacuum exposition we reveal the presence of non-perovskite components with a simple inspection of the morphology of the layer; all experiments are supported by X-ray and electron diffraction measurements. Besides degradation, we discuss recrystallization and propose post-crystallization to explain the experimental results. This physical approach towards perovskite layers with large grains by post-processing is a key step towards large-area preparation of high-quality layers for device manufacturing.

Keywords Thermal imprint · Methylammonium lead bromide · Layer upgrade · Vacuum exposition · Recrystallization · Physical concept

✉ Andre Mayer
amayer@uni-wuppertal.de

[1] Chair of Large Area Optoelectronics, School of Electrical, Information and Media Engineering, University of Wuppertal, Rainer-Gruenter-Str. 21, 42119 Wuppertal, Germany

[2] Chair of Electronic Devices, School of Electrical, Information and Media Engineering, University of Wuppertal, Rainer-Gruenter-Str. 21, 42119 Wuppertal, Germany

[3] Institute of Particle Technology, University of Wuppertal, Rainer-Gruenter-Str. 21, 42119 Wuppertal, Germany

[4] Chair for Novel Manufacturing Technologies and Materials, University of Wuppertal, Bahnhofstr. 15, 42651 Solingen, Germany

[5] School of Electrical, Information and Media Engineering, University of Wuppertal, Rainer-Gruenter-Str. 21, 42119 Wuppertal, Germany

1 Introduction

The properties of semiconducting organic–inorganic perovskites are remarkable. Some representatives of this class combine two key qualifications, referring to the processing capabilities on the one hand and the physical properties on the other hand. The possibility to prepare them from a solution-based process opens the door to the mass production of devices at low cost. The direct band gap [1] qualifies them for technical applications with optical devices. The bandgap is in the visible regime and can be tuned by the composition of the perovskite [2]. These materials are highly interesting for the development of thin film solar cells, a field, where in recent years remarkable energy conversion efficiencies have been reported [3, 4]. A further field of application are LEDs [5], lasers [6] and sensors [7].

One of the milestones in the manufacturing of large-area perovskite devices is the changeover from lab processing to a processing that is up-scalable and works under ambient atmosphere. Promising candidates for layer deposition are slot die coating [8][8] or ink jet printing [10]. One requirement to these films in general is a high homogeneity so that a well-defined interface to the subsequent layer is provided. Furthermore, the layer should be free from pinholes, which may lead to shorts. Most often homogeneous layers with large crystals are beneficial for optimum device performance. To achieve this on large areas conventional concepts like e.g. anti-solvent treatment [11, 12] for fast and uniform crystallization at the lab scale may have to be reconsidered [9, 13].

The process window for successfully preparing methylammonium-based perovskites is relatively narrow [14]. According to our experience, small variations of the process may end up in the complete loss of a batch of samples. Generally, the definition of a process window is a question of the knowledge on and the experience with the processes, the materials and the machines used and, in addition, of the specific material properties envisaged for a certain application. We want to keep the findings close to praxis and will present a quite detailed discussion of our experiments to render this investigation comprehensible. The conclusions refer to basic thermodynamic data of the materials involved that are generally available. In this way the results can easily be transferred to other processing scenarios and may help to proceed from lab-scale to large-area processing of perovskite layers for manufacturing by simply assembling individual pieces of the puzzle in a detective way.

Our approach is to start with imperfect layers (highly unsatisfactory with respect to devices) and to 'upgrade' them by post-processing, a simple means to decouple film quality from the initial deposition process. Different from a recent approach [14], our upgrading works with a thermal imprint step. It has already been shown by X-ray diffraction (XRD) [6, 15, 16] that thermal imprint is best suited to improve the crystal size of I- and Br-based perovskite layers, thereby improving their optical properties as well [6, 15]. For this purpose, the layer is covered with a flat stamp and treated with temperature and pressure. An adequate imprint temperature is 150 °C which is markedly higher than usual annealing temperatures for perovskite layers [17, 18]. So far it seems that during imprint the stamp protects the layer from the surrounding atmosphere and avoids the evaporation of volatile components, thus hindering degradation. In this way the influence from the outside can be well controlled. However, we use a relatively high temperature that may promote undesired processes inside the perovskite. In the best-case impurities may precipitate at the grain boundaries, in the worst case non-reversible chemical reactions may occur and result in degradation.

A closer look at the reaction equation for the formation of the perovskite helps to discuss the situation. We decided to use a methylammonium (MA)-based perovskite; its limited stability with temperature is challenging. The choice for the halide component was Br, namely methylammonium bromide (MABr); the respective Br-based perovskite features no phase transition in the temperature regime under investigation (up to 200 °C). In view of device manufacturing, lead acetate ($Pb(AcO)_2$), namely lead acetate trihydrate ($Pb(AcO)_2\ 3H_2O$) was used as the Pb-containing precursor component, a low-price alternative to conventional lead bromide ($PbBr_2$). However, in case of the trihydrate the presence of water, a strong complexing agent [19], represents an intricate impurity which may contribute to degradation as addressed below. In summary, under stoichiometric conditions our perovskite formation can be described by the following equation,

$$3\mathrm{MABr} + \mathrm{Pb(AcO)_2 3H_2O} \rightarrow \mathrm{MAPbBr_3} + \mathrm{R}\left(2\mathrm{MA},\ 2\mathrm{AcO},\ 3\mathrm{H_2O}\right), \quad (1)$$

where $MAPbBr_3$ is the intended perovskite and R(2MA, 2AcO, $3H_2O$) denominates some rest (R), namely potential products formed by the surplus of MA ($CH_3NH_3^+$), AcO (CH_3COO^-) and water. By deprotonation/protonation MA and AcO transform into methylamine, MMA (CH_3NH_2) and acetic acid, AcOH (CH_3COOH), quite stable compounds. Though less probable at first glance, reaction of Ac to MAAc ($CH_3NH_2{\cdot}CH_3COOH$) is also reported in perovskite literature [20, 21]. When the stoichiometry is violated or when the conversion of precursor into perovskite is incomplete the layer will, in addition, contain some amount of one or both precursor components, most probably dissociated into their ionic constituents. Then Pb^{++}-ions may combine with OH^- (from AcOH formation) to form $Pb(OH)_2$ (or rather the hydrated oxide $PbO{\cdot}H_2O$) which is also noted as a light-induced degradation product of Pb-based perovskites [22]. Water (together with DMF) may stabilize all ionic components present as complexes [19].

Concerning degradation, stability of these perovskites is a further issue. An important and well-known chemical degradation mechanism of methylammonium-based perovskites under ambient conditions can be attributed to an acid–base reaction of the MA component in the perovskite which is deprotonated to MMA by a base. The missing MA-ion leads to a decomposition of the respective perovskite unit where at the end $PbBr_2$ remains as a solid component, only. Besides OH^- [23], a base in question that is reported in literature is H_2O [24]; adopted to our perovskite the degradation then proceeds according to

$$\mathrm{MAPbBr_3(s)} + \mathrm{H_2O(g)} \rightarrow \mathrm{MMA(g)} + \mathrm{HBr(g)} + \mathrm{PbBr_2(s)} + \mathrm{H_2O(g)}. \quad (2)$$

Accordingly, trace amounts of water (humidity) attack the methylammonium in the perovskite and act as a catalyst for this reaction; however, a surplus of water will lead to the dissolution of the gaseous components to MMA(aq) and HBr(aq) (for details see the referenced literature).

In the absence of proton transfer an alternative water-induced degradation concept is reported that is based on the progressive hydration of the perovskite crystal [25]. In the first instance, the formation of a mono-hydrate increases the lattice constant, a still reversible process. Subsequent formation of a di-hydrate already represents a partial destruction of the perovskite unit and will be irreversible, at least in parts. Three H_2O -molecules per perovskite unit represent a threshold for dissolution. With our Br-based perovskite and a surplus of water the degradation reaction then reads

$$MAPbBr_3(s) + H_2O(l) \rightarrow MABr(aq) + PbBr_2(s) + H_2O(l), \quad (3)$$

resulting in somewhat differing degradation products. It is noted [25] that this reaction is irreversible as the MABr stays in solution, whereas $PbBr_2$ may precipitate as a solid thus hampering a later re-formation of the perovskite. As it is also known that water as a highly polar solvent forms stable complexes with these polar components [19] (which are often used as precursor materials) the $PbBr_2$ may stay in solution, too.

To summarize, potential (side) products resulting from the water-induced degradation of the perovskite are MMA, HBr, $PbBr_2$ and, in case of severe water attack, MABr. Besides MABr, these decomposition products are also reported with a purely thermal degradation [26]. With our experiments, thermal degradation as well as water-induced degradation is an issue, due to the ambient-near conditions under imprint and due to the trihydrate as a precursor component.

Common solvents for MA-based perovskites are dimethylformamide (DMF), dimethyl sulfoxide (DMSO) and N-methyl-2-pyrrolidone (NMP). Similar to water, these solvents may form complexes with the precursors [3]. Depending on the soft-bake temperature residuals of these complexes may remain in the perovskite. DMF, the solvent used here, features a reduced tendency to form complexes compared to DMSO and NMP [27].

Important thermodynamic data (melting point, boiling point and vapour pressure) of all components of interest are summarized in Table 1 indicating, in addition, the physical phase at the temperatures and pressures characteristic of our investigation, at the soft-bake temperatures T_{SB} (referring to preparation of the pristine layers) and the imprint temperature T_i (referring to the upgrade), as well as under exposition to vacuum (VAC, referring to the status/consistence testing).

Table 1 Thermodynamic properties of precursors, products, side-products and common solvents involved in the preparation of $MAPbBr_3$ from MABr and $Pb(AcO)_2$ as well as their physical phase at characteristic temperatures and pressures

	Compounds	Phase transitions			Phase at				
		T_M/°C (1 bar)	T_B/°C (1 bar)	p_V/mbar (20 °C)	RT (25 °C)	T_{SB1} (75 °C)	T_{SB2} (125 °C)	T_i (150 °C)	VAC (10^{-3} mbar)
Precursors	MABr	247.35 [28]	Dec [28]	10^{-7} [28]	s	s	s	s	s
	$Pb(AcO)_2$	280*	Dec	–	s	s	s	s	–
	$Pb(AcO)_2$ $3H_2O$	75*	Dec	<0.1 [29]	s	–	–	–	g
Products	$MAPbBr_3$	–	–	–	s	s	s	s	s
	MMA	−93.5	−6.3	3.1×10^3	g	g	g	g	g
	AcOH	17	118	14.3	l	l	g	g	g
	H_2O	0	100	23.4	l	l	g	g	g
Side-products	MAAc	75 [30]	Dec [31]	4 [30]	s	l	–	–	g
	$Pb(OH)_2$	145**	Dec	–	s	s	s	–	–
	$PbBr_2$	371	892	1.2×10^{-17}	s	s	s	s	s
	HBr	−86.8	−66.4	2×10^4 [32]	g	g	g	g	g
Solvents	DMF	−60.5	153	3	l	l	l	l /g	g
	DMSO	17.9	189	0.59	l	l	l	l	g
	NMP	−23.1	202	0.32 [33]	l	l	l	l	g

Nomenclature: T_M = melting point, T_B = boiling point, T_{SB1} and T_{SB2} = soft-bake temperatures, T_i = imprint temperature, p_v = vapor pressure, VAC = vacuum, Dec = decomposition, – = not applicable/no specification possible

*Dehydration at already about 50 °C and a beginning decomposition at 200 °C are also reported [34, 35]

**Dehydration (abstraction of water) at 130 °C and decomposition at 145 °C are also reported [36]

References: with the exception of the given references all values are taken from the CRC Handbook [37]

Table 1 was used to design the experiments and to discuss the respective results.

Table 1 is of central importance for our approach. Thermodynamic data are available for almost any material of interest in context with perovskite preparation (precursors, products and side products, solvents) and are assembled in a facile way accounting for the preparation conditions in mind (e.g. temperatures of soft-bake and imprint). As we discuss our results first and foremost by referring to these thermodynamic data a transfer to other situations is straightforward. As to start we support our arguments by electron and X-ray diffraction measurements, techniques less suited for inspection with large-area processing. However, our physical approach based on thermodynamic data is largely independent from scaling.

To complement Table 1, the general thermal behaviour of the perovskite itself, $MAPbBr_3$, was characterized by a thermo-gravimetric analysis (TGA). Figure 1 gives the decrease in the relative mass, $m_{SC,R}$, with temperature and its respective derivation, $dm_{SC,R}/dT$, as obtained with a single crystal. The mass loss proceeds in two steps, a first step from 100 to 76% and a second step from 76 to 0%. The first step of about 24% corresponds to the methylammonium content of the perovskite (molar masses: $M_{MABr} = 111.97$ g/mol [38], $M_{PbBr2} = 367.05$ g/mol [39]). The respective thermal event (dip at 383 °C) can be linked with the melting of $PbBr_2$. Decomposition is negligible up to more than 250 °C (2% weight loss at 320 °C). Thus, the perovskite is solid in the temperature regime under investigation (see Table 1) but completely decomposes before any phase transition is reached, in good accordance with the literature [40, 41].

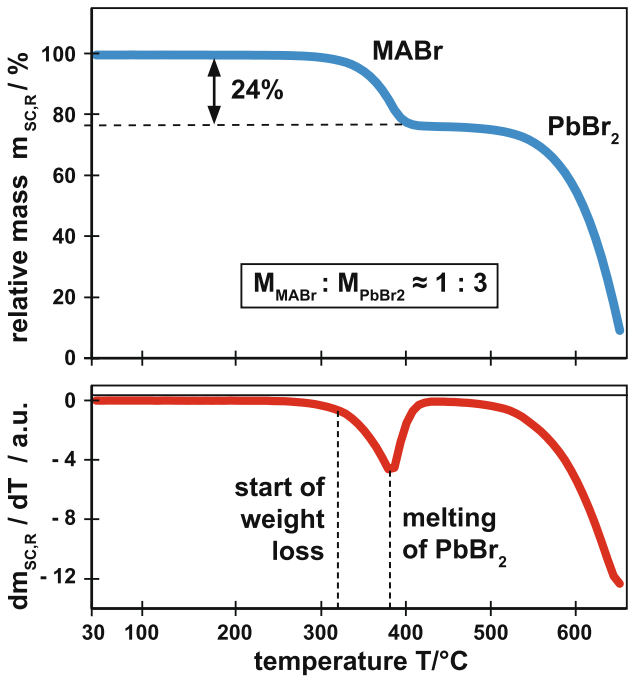

Fig. 1 TGA measurement with $MAPbBr_3$ single crystal (heating rate: 10 °C/min). The loss of the relative mass, $m_{SC,R}$, against temperature (top) and the respective derivation (bottom)

The focus of the actual study lies on the physical processes involved in upgrading a methylammonium-based perovskite layer by post-treatment via thermal imprint. For this study, pristine layers with different composition/side-products and crystal size are provided by varying the respective soft-bake temperature after spin-coating. During imprint a relatively high temperature of 150 °C is applied which otherwise would stimulate a decomposition of the material. The status of the upgraded layers is addressed by exposing the imprinted samples to vacuum; an inspection of the morphology then provides a simple means to indicate non-perovskite constituents, avoiding sophisticated characterization techniques. A special imprint technique, 'hot loading', allows to observe the response of the perovskite layer at one specific temperature, excluding heating and cooling phases; in the actual investigation it is used to assess the temporal response of the pristine layer to the imprint temperature and to develop a physical concept of the processes involved during upgrading. The suitability of lead acetate as a cost-efficient precursor material, in particular in case of the trihydrate, is critically discussed.

In contrast to the multitude of chemical strategies reported in literature the actual investigation represents a physical approach towards high-quality perovskite layers that is up-scalable, namely upgrading by thermal imprint. Based primarily on the thermodynamic data of the materials involved it can easily be transferred to other processing situations and/or other materials;—as to start, electron and X-ray diffraction measurements provide evidence for our argumentation. In addition, processing largely proceeds under ambient atmosphere. This engineering approach may contribute to pave the way for the reproducible manufacturing of devices based on perovskite thin films in the future.

2 Experimental

The perovskite layers were prepared in a solution-based process under a protective N_2-atmosphere. A solution according to Ref. [6], consisting of 504 mg MABr (Dyesol), 569 mg lead acetate trihydrate, $Pb(AcO)_2\ 3H_2O$ (purity 99.999%, Sigma-Aldrich) and 1 ml anhydrous dimethylformamide, DMF (purity 99.99%, Sigma-Aldrich) was prepared. This corresponds to a molar mass ratio of MABr: $Pb(AcO)_2$ of 3:1, a stoichiometric mixture, being commensurate with the envisaged perovskite. The solution was stirred for about 24 h at a temperature of 60 °C. Then the layer was deposited by spin coating (5000 rpm, 3 min, room temperature) and afterwards soft-baked for 2 min. The soft-bake temperature was varied from 75 to 200 °C. As the layer morphology varies

from batch to batch, only samples from the same batch were compared. The substrate material was Si. Before deposition the substrates were cleaned in citric acid, deionized water and isopropanol for 15 min, each under ultrasonic agitation.

For the imprint experiments a proprietary three-column imprint system was used [42, 43]. The process flow is indicated in Fig. 2. Our conventional imprint process for $MAPbBr_3$ layers (see blue curve) starts with the loading of the machine with the imprint stack (sample and stamp), directly followed by the application of the full imprint pressure, $p_i = 100$ bar; the pressure remains constant during the entire process. Then the imprint system is heated up to the imprint temperature, T_i. When the imprint temperature is reached it is kept constant for an imprint time of $t_i = 5$ min, followed by cool-down. At room temperature the pressure is released and the system is unloaded. When a flat stamp (e.g. a piece of Si) is used, as it is the case here, we call this process 'planar hot pressing', PHP [18]. The flat Si stamps used were covered with a chemically bound anti-sticking layer of a fluorinated trichlorosilane (44831, Merk) from the gas phase [44]. The imprint temperature was 150 °C; for investigation reasons also an imprint at 75 °C was performed here. Typically, the system heat-up takes about 10 min for an imprint temperature of 75 °C and 20 min for an imprint temperature of 150 °C [45]. The cool-down to room temperature takes less than 2 min due to efficient water cooling.

In order to allow the correlation of an imprint result obtained for the perovskite layer with a well-defined imprint temperature a specific technique was used, 'hot loading' (HL), as also indicated in Fig. 2 (see red curve). This simply means that we loaded the imprint system after heat-up only, with any temperature under investigation. For short time experiments also the cool-down of the system was skipped and the sample was unloaded after pressure release. This

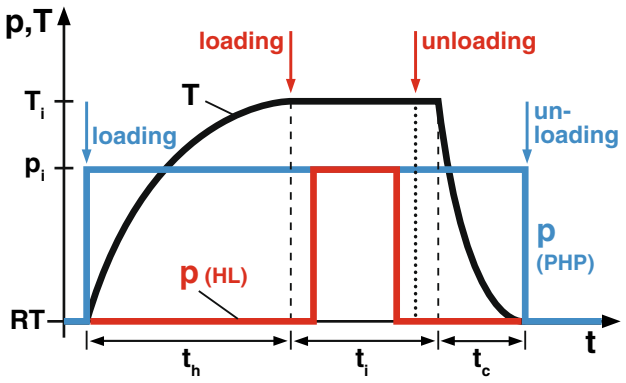

Fig. 2 Process flow for the upgrade of perovskite layers by imprint. Blue curve: pressure characteristics for conventional imprint (planar hot pressing, PHP). Red curve: pressure characteristics for hot loading experiments (HL) (p_i = imprint pressure, T_i = imprint temperature, t_h = heat-up time, t_i = imprint time, t_c = cool-down time, RT = room temperature)

further reduces the actual cool-down time for the sample to some seconds.

The imprint system used operates under ambient conditions and features 150 mm diameter hotplates, much larger than the samples imprinted. Hence, before loading the imprint stack (sample and stamp) was wrapped together into a double sachet from Al foil. The foil consists of 30 µm thick pure Al (EN-AW1050A, Alujet-Universal GmbH). The inner sachet contains the imprint stack, only. The outer sachet, in addition, binds the sandwich of the inner sachet together between two heat conducting foils (KU-CG30/R, 200 µm thick, Boyd Corporation GmbH). The Al and the heat conducting foils form a cushion layer that largely compensates the unevenness of the hotplates and the imprint stack as well; in this way a most homogenous distribution of the imprint pressure is assured. The main benefit of this technique for the actual investigation is that the sachet represents a portable, well-assembled imprint stack that is swiftly and precisely loaded to and unloaded from the imprint system; loading of the sachet to the correct position and pressure application take 20–30 s, only. This is the basis for short-term imprint experiments under hot loading; the minimum imprint time investigated was 30 s. A further benefit of the sachet is that it can be prepared under any condition desired (e.g. cleanroom, ambient conditions or N_2 atmosphere);—as we aim at atmospheric processing our sachet was prepared under ambient conditions. As assembly of the inner sachet takes about 1 min, the free contact of the perovskite layer to ambient atmosphere is limited. However, we expect a monolayer of humid air on our samples before imprint (comparable to loading under fully atmospheric conditions).

The substrate size was 2.5×2.5 cm^2. To keep the experiments as convincing and as sound as possible, we cleaved a small part from each sample (≈5 mm wide strip). This small part was held under dry nitrogen and served as a reference for a later inspection of the pristine layer. The stamp had a size of 2×2 cm^2, slightly smaller than the remaining sample size.

We tested the overall consistence/status of our perovskite layers in the way that the imprinted samples were held under vacuum ($p_{vac} \approx 10^{-3}$ mbar) for a duration of 1 to 7 days;—it is known from literature that the exposure to high and ultrahigh vacuum results in a slow degradation of MA-based organic–inorganic perovskites which is substantially accelerated under temperature or irradiation (light, X-rays) [22, 23, 46, 47]. In our case of a medium to rough vacuum only, in dark and at room temperature, vacuum-induced degradation is negligible; vacuum exposition simply results in the evaporation of components embedded in the layer that are volatile at the respective pressure.

The morphology of the samples was characterized by scanning electron microscopy, SEM (S-FEG XL 30 S, Thermo Fisher Scientific). An evaluation of SEM

micrographs with respect to the size of grains and holes was performed with the help of Fiji, an open-source software for image processing. XRD (X-ray diffraction) measurements (Bruker D2 Phaser) and EDX (electron diffraction) measurements (FEI Quanta 450 FEG with EDAX Si(Li)-EDX detector) were performed to further characterize the layer status; these supplementary measurements are detailed in the supporting information.

3 Results and discussion

3.1 Pristine layer

Our focus is an upgrade of the perovskite layer by thermal imprinting, and one issue in this context is the impact of the preparation conditions of the starting layer on upgrading. After imprint the layer should be pinhole-free, with a high degree of crystallinity and a low amount of side-products precipitated in the grain boundaries as it is required for most applications [3].

To assess the consistence of the starting layer we varied the temperature of the soft-bake following spin-coating; during soft-bake the perovskite is formed from the precursor components. Accordingly, we chose a temperature window based on the properties of the precursor lead acetate—MABr is not critical (Table 1). At the minimum temperature of 75 °C the $Pb(AcO)_2$ $3H_2O$ melts and dehydration is not yet complete [35]; at the highest temperature of 200 °C the $Pb(AcO)_2$ itself begins to decompose [34]. Furthermore, as our precursor contains water, a soft-bake temperature of 100 °C represents a threshold when preparing layers with or without water.

Figure 3 documents the results. Crystal growth with temperature is evident, as it is expected quite generally with polycrystalline layers [48]. An almost continuous layer is obtained with a soft-bake temperature in the range of 100 °C–125 °C. When the soft-bake temperature is lower the samples often feature just small grains and are porous. These small grains have a relatively high potential to grow during imprint; an upgrade of these layers with respect to grain size by imprinting is quite likely. At higher soft-bake temperatures thermal degradation occurs; the grains are larger and due to crystal growth in three dimensions, the layers become thickness-modulated, terraces and micron-sized pinholes develop. We found that holes of that size cannot be closed during post-treatment by thermal imprinting. Thus, for our experiments with the trihydrate as a precursor component we choose layers obtained with a soft-bake temperature of 75 °C and 125 °C, namely pristine layers that may contain water and others that should be largely water-free.

Our typical imprint temperature is 150 °C. This is well below any starting mass loss due to a decomposition of the single crystal (see Fig. 1). However, the temperature response of the polycrystalline layers is more delicate, due to the presence of grain boundaries and potential (side-) products. Therefore, the choice of the imprint temperature should consider annealing experiments (as those in Fig. 3) in addition to the TGA-analysis. A close inspection of the layer obtained at a soft-bake temperature of ≥150 °C not only reveals pinholes, but also some non-perovskite material between the large grains (see arrows), as also sometimes reported in literature as a 'secondary phase' [49] or an 'intermediate phase' [50]. Such features indicate degradation as well as temperature/solvent-induced deficiencies in perovskite formation. We deliberately choose an imprint temperature at which, even under N_2 atmosphere, the polycrystalline layer is already adversely affected. As a compromise with the overall processing time (—high temperatures require a long heat-up—) we decided to upgrade the polycrystalline perovskite layers by imprinting at 150 °C, a temperature higher than the soft-bake temperatures chosen, relying on the protective effect of the stamp.

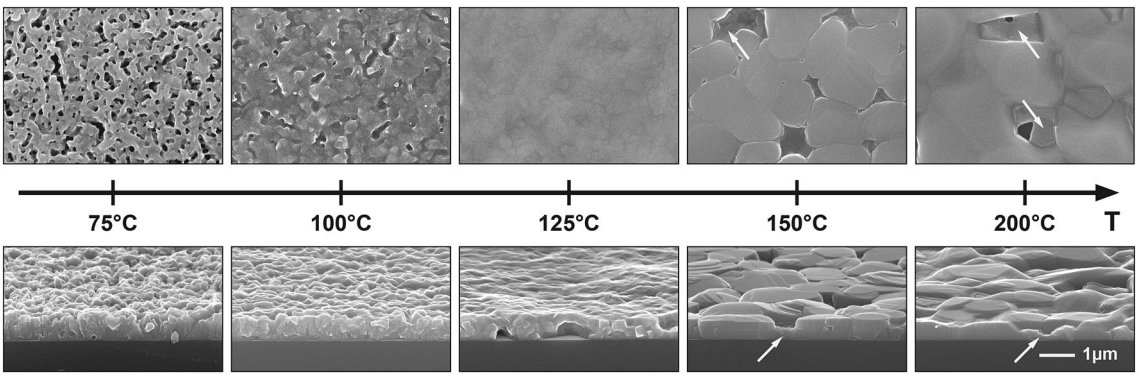

Fig. 3 Pristine layers of $MAPbBr_3$ obtained at different soft-bake temperatures, top view and cross sections (soft-bake time 2 min, N_2 atmosphere). Arrows: see text

It was found that the pristine layers may exhibit major differences from batch to batch, despite the always similar preparation. Further analysis by XRD showed that the main peaks are well assigned to the envisaged perovskite (see Fig. S-A1); some minor peaks (Fig. S-A2) may indicate precursor rests like $Pb(AcO)_2$ or MABr. In addition, EDX analysis was performed; against expectation an atomic ratio of Br: Pb ≈ 3.5: 1 was found (Fig. S-B1, Tab. S-B5). Close inspection of the preparation process revealed that the surplus of Br in the layers may result from incomplete dissolution of the precursor, as solid remnants were found in the preparation flasks.

Figure 4 documents the pristine status after soft-bake at 150 °C exemplary by SEM micrographs taken with a BSE detector (backscattered electrons), indicating local differences in composition. The bright grains (high mean atomic number) of Fig. 4b designate the perovskite crystals. The dark grain boundaries (lower mean atomic number) indicate a surplus of Br there; this becomes even more obvious when the layer is prepared with a deliberate surplus of Br (Fig. 4c). With our perovskite layers and the equipment used, a local EDX analysis to characterize the atomic composition is limited; at a magnification too large (required to analyse a single grain) the perovskite becomes degraded by the electron irradiation (see Fig. S-B2); nonetheless, the higher Br content in the inter-grain position (Fig. S-B2d) compared to the grain clearly indicates a non-perovskite material there (see also arrows in Fig. 3). As a consequence, we had to learn that our layers prepared with a molar ratio of the precursors of 3:1 and following the procedure indicated in the experimental part will feature a surplus of Br (3.5:1), located primarily at/near the grain boundaries.

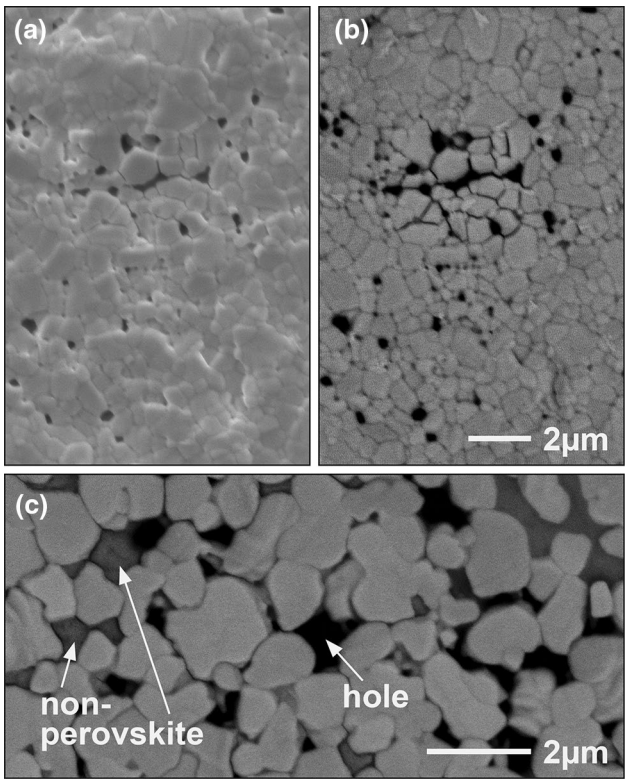

Fig. 4 Local composition of pristine layers, taking the example of a sample prepared at a soft-bake temperature of 150 °C. SEM secondary electron micrograph (**a**) and backscattered electron micrograph (**b**) taken from the same location; the latter is indicative for the mean atomic number of the constituents. **a**, **b** refer to the stoichiometric mixture as explained in the experimental part; **c** refers to a non-stoichiometric mixture containing a surplus of the Br-precursor (backscattered electron image)

3.2 Hot loading experiments

3.2.1 Experimental results

In order to investigate the layer upgrade at 150 °C we performed hot loading experiments (no heat-up, no cool-down); Fig. 5 documents the key findings. The left column refers to layers prepared with a soft-bake at 75 °C and the right column refers to layers prepared with a soft-bake at 125 °C. Panels a/b) show the respective pristine layers, panels c/d) and e/f) are typical of the layers after an imprint time of 30 s and 30 min, respectively.

To characterize the layers, the grain size (lateral dimension of continuous crystalline regions) was evaluated from SEM micrographs; the results are summarized in Table 2. Compared to the pristine layers, the grain size has already increased by a factor of >5 after 30 s of imprint. During the following almost 30 min of imprint time, further growth by a factor of 2–3 is observed, only. Obviously, the main grain growth occurs within the initial minute (20–30 s for loading plus 30 s of imprint); extending the imprint duration is not too significant to increase the grain size. However, after 30 min the grain size is almost a factor of two larger with the samples prepared at the higher soft-bake temperature. From supplementary XRD measurements (see Fig. S-A3) an increase in the relative crystalline area with increasing imprint time is obvious (less grain boundaries), the degradation remaining negligible (Fig. S-A4).

As also evident from Fig. 5, holes have developed during crystal growth as well. These holes were found to be symptomatic of preparing Br-based perovskites; in this respect I-based perovskites seem to be much less susceptible [18]. (We denominate any recess from the top level of the imprinted layer as a 'hole'. These holes may be empty or filled up to some level.) At first glance the holes seem to grow with increasing imprint time. However, tracking of the overall area occupied by holes over the time span from 30 s to 30 min of imprint reveals that the mean overall hole area remains largely constant. As summarized in Table 2, it is somewhat larger with a soft-bake at 75 °C than with 125 °C. With a 75 °C soft-bake the holes make up 5.5%,

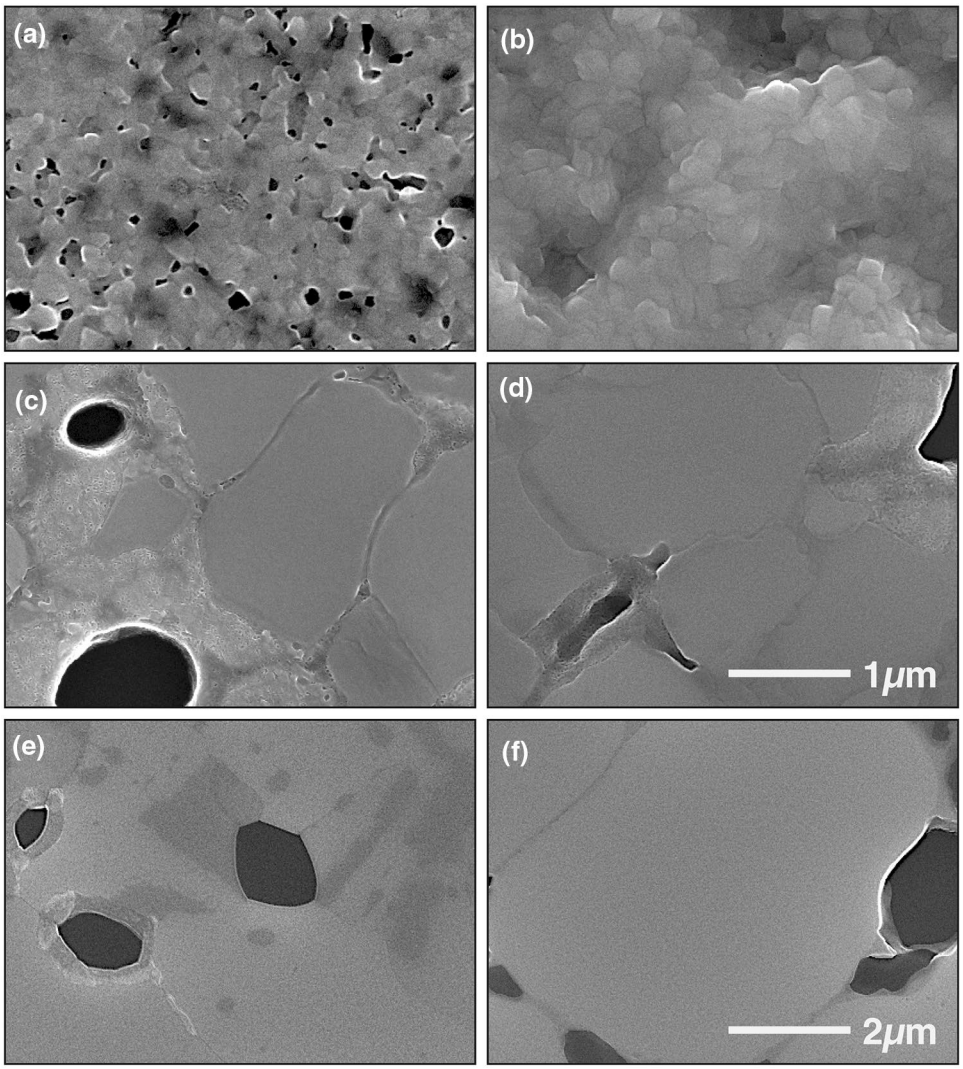

Fig. 5 Perovskite layers prepared at different soft-bake temperatures, observed after different imprint times (hot loading experiment). The soft-bake temperature is 75 °C (left column) and 125 °C (right column). The imprint was performed at 150 °C with a pressure of 100 bar, followed by vacuum exposition for about 1 day. **a**, **b** Pristine layers; **c**, **d** imprint time: 30 s; **e**, **f** imprint time: 30 min. The scale bar is similar with (**a**) to (**d**) and with (**e**, **f**). In order to pinpoint the details of the porous regions, only small sections of the sample are shown; evaluation of the mean values given in Table 2 was performed from survey micrographs

Table 2 Evaluation of the experiment of Fig. 5 (hot loading at 150 °C) from survey SEM micrographs; mean values and their respective root mean square variations (in brackets)

Upgrade at $T_i = 150$ °C	$T_{SB1} = 75$ °C	$T_{SB2} = 125$ °C
Grain size		
pristine	0.22 µm (±18%)	0.24 µm (±25%)
$t_i = 30$ s	1.2 µm (±32%)	1.3 µm (±30%)
$t_i = 30$ min	2.5 µm (±17%)	4.1 µm (±30%)
Hole area		
$t_i = 30$ s to 30 min	5.5%	4.1%

'Grain size' refers to the lateral dimension of continuous crystalline regions; 'hole area' is given as the overall area occupied by empty or partly filled holes per reference area analysed (≈1400 µm^2, 50 µm × 28 µm), characterized by a recess with respect to the top level of the imprinted surface

The relatively high standard variations just indicate that the dimensions of the grains feature a relatively broad distribution;—the mean values (and standard deviations) evaluated from different micrographs are highly comparable

with a 125 °C soft-bake 4.1%, relative to the overall area, only.

Furthermore, detailed inspection reveals a porous or grainy region at grain boundaries and surrounding the holes. It is most pronounced with the experiment at the short imprint time and the low soft-bake temperature (Fig. 5c); with increasing imprint time the width of this region shrinks to a small rim around the holes or has completely vanished (Fig. 5e). With the higher soft-bake temperature (125 °C) the porous rim is less pronounced, see panels (d) and (f); after 30 s of imprint, it is just narrow and again decreases in width with increasing imprint time. After an imprint for 30 min the porous region has completely disappeared.

Our impression is that the holes and porous or grainy regions observed after vacuum exposition must result from an evaporation of impurities, namely non-perovskite excess material still present in the layers after upgrading via imprint;—except MABr, $PbBr_2$ and the perovskite itself all components involved are gaseous (or decomposed) under

vacuum (see Table 1); in fact, some evaporation is in accord with XRD analysis, without affecting the integrity of the crystal (see Fig. S-A5/6); EDX reveals a loss of Br upon vacuum exposition, again indicating evaporation (see Tab. S-B6). As recrystallization goes hand in hand with purification,—impurities are expelled from the growing grains [48]—, the excess material accumulates at grain boundaries and grain boundary junctions. With ongoing grain growth, the overall length of the grain-boundaries decreases; this is in accord with holes of growing size but decreasing density, as documented by the overall area occupied by holes which remains largely constant during recrystallization (Table 2); the excess material contained in the layers is mainly rearranged between the growing crystalline regions.

The question is, what this excess material is. Some excess material is already present in the pristine layers after soft-bake;—this may be more critical with the lower soft-bake temperature. However, excess material may also form during the upgrading step at elevated temperature. In order to eliminate thermal degradation a special hot loading experiment was performed at an imprint temperature as low as 75 °C; of course, this does only make sense with $T_{SB1} = 75$ °C, so that the sample has already been exposed to its maximum processing temperature during soft-bake. At this low temperature grain growth during imprint is low [51] and temperature-induced degradation is negligible. In order to achieve still a high degree of dehydration (with $T_{SB1} = 75$ °C the layer will contain water) and to give any excess material enough time to aggregate near grain boundaries we ran this control experiment with an imprint time as long as 1 h. One half of the sample was stored in vacuum for one week and the other half was held under nitrogen to serve as a reference. SEM inspection was performed directly after imprint and after the 1-week storage.

The main results are shown in Fig. 6. Despite the low temperature the grains have grown by a factor of 3.5; after imprinting, the average grain size of 170 nm (±38%) with the pristine layer increased to 600 nm (±31%) and holes occupying 9% of the overall area developed. A cross section of the layer directly after imprint is presented in Fig. 6a. No porous region is observed and the 'holes' are completely filled with some non-perovskite material. The morphology after N_2-storage is similar. However, after vacuum exposition the morphology has changed, see Fig. 6b, c. Both, the top view and the cross section of the sample clearly show the porous rim around the holes again, as well as some solid residual within the holes, resembling the residual observed in holes of the pristine layer (see Fig. 3, 4) referred to as 'non-perovskite' material. Figure 6d) shows regions with a rather grainy, porous structure between grains for a sample taken from a different batch; EDX analysis (Fig. S-B3) indicates a low Br content there (most likely $PbBr_2$, as also reported in literature [23]), whereas the solid material in the holes features an intermediate Br content (potentially a mixture of $PbBr_2$ with Br or Br-compounds), again quite similar to the findings with the pristine layer (Fig. S-B2).

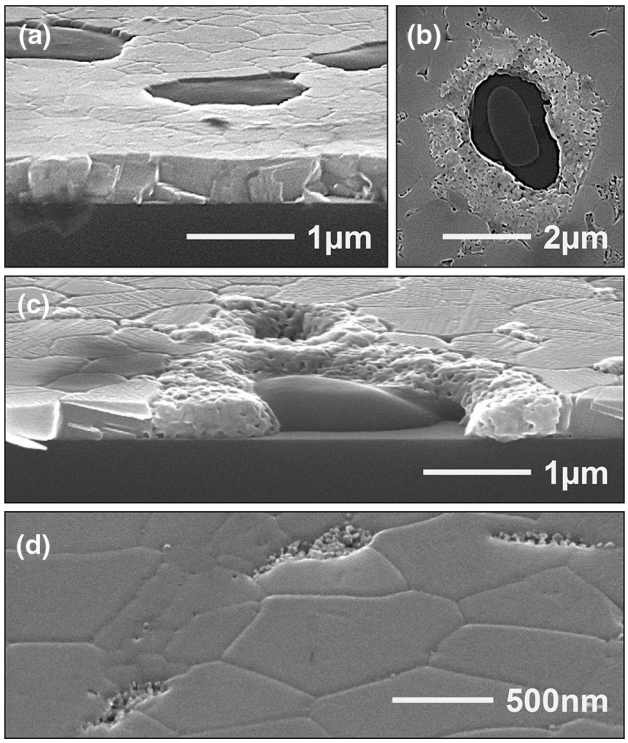

Fig. 6 Control experiment with hot loading at $T_i = 75$ °C ($t_i = 1$ h), with a pristine layer soft-baked at $T_{SB1} = 75$ °C. **a** Cross section of the perovskite layer directly after imprint, **b**, **c** top view and cross section of the sample after one day of vacuum exposition. **d** Sample with grainy, porous regions between grains, taken from a different batch

The existence of holes (possibly with some solid residual) and porous or grainy regions is largely independent from the elevated temperature during upgrade (see Figs. 5 and 6). In addition, Fig. 6a) documents that directly after imprint the final holes were filled with some material that evaporated in parts afterwards. With respect to our question on the origin of this excess material the control experiment tells us that it must have already been present in the pristine layer, at least with $T_{SB1} = 75$ °C. Moreover, an upgrading at elevated temperature rather seems to decrease the amount of excess material; the overall hole area is smaller when imprinted at 150 °C (4.1% and 5.5%, Table 2 and Fig. 5) than with an imprint at 75 °C (9%, Fig. 6), and the porous or grainy regions are less pronounced.

3.2.2 Excess material

Next, potential excess materials contained in the layers after soft-bake and after imprint, acting as impurities in the perovskite, will be discussed. The discussion is based on the thermodynamic data summarized in Table 1. However, with

the ionic mixture present complex formation of DMF and water with the ionic components may impede evaporation of liquid constituents.

i. It could be the solvent used, here DMF. Compared to other solvents common with perovskite preparation DMF has a relatively high vapour pressure, so that a part of the solvent should be vapourized after spin-coating; nevertheless, residual solvent (in particular with complexes) cannot be excluded, especially with $T_{SB1} = 75$ °C. At imprint temperature (150 °C) DMF starts to become gaseous.
ii. (Side-)products from perovskite formation are also conceivable, originating from the surplus of methylammonium (MA) and acetate (AcO), see Eq. 1. In the form of methylamine (MMA) the MA-component would have left the layer during soft-bake. Acetic acid (AcOH) is still liquid at T_{SB1} but gaseous at T_{SB2}. Thus, we expect some residual AcOH with the samples prepared at a soft-bake temperature of 75 °C. In case that the acetate MAAc is formed this side-product will be liquid during soft-bake at T_{SB1} and will remain in the layer. As it decomposes around 90 °C, layers prepared at T_{SB2} should not contain MAAc. If present, $Pb(OH)_2$ (or $PbO{\cdot}H_2O$) will stay in the layers, with both soft-bake temperatures. After all, bromine will contribute to the excess material, according to our EDX results (Fig. S-B1, Tab. S-B5). In the form of solid MABr or when dissociated and/or dissolved/bound in complexes it will still be present after soft-bake.
iii. Furthermore, side-products resulting from thermal decomposition or perovskite degradation [24] come into play. Existing $Pb(OH)_2$ will decompose/dehydrate (see Table 1) at upgrading temperature, resulting in PbO and H_2O. $PbBr_2$ (see Eq. 2) is solid and will stay in the layer, as already obvious from the TGA measurement (Fig. 1). HBr is gaseous and will evaporate as long as it is not hindered by the stamp. Water-induced degradation leading to MABr may also be an issue with sample preparation at $T_{SB1} = 75$ °C (see Fig. S-A4). (—We do not expect degradation according to Eq. 3 to occur throughout the layer; however, it may occur locally as discussed below.)
iv. After all, as our layers are prepared from a trihydrate, water takes on a specific role. As already addressed it is able to form hydrates with the perovskite [52]. So, with a layer prepared at a soft-bake temperature of $T_{SB1} = 75$ °C the water contained may partly be integrated in the crystal grains of the pristine perovskite layer; however, at our imprint temperature of 150 °C any hydrated perovskite crystal will dehydrate. In contrast, with the pristine layers obtained at $T_{SB2} = 125$ °C hydration should not be a major issue [35]. In particular, water molecules are known to form relatively stable complexes with the ionic components of the precursor [53]; complex formation may postpone evaporation to higher temperatures, so that even at $T_{SB2} = 125$ °C some water complexes may remain.

To summarize, we expect pristine layers prepared at $T_{SB1} = 75$ °C to contain DMF, AcOH, MAAc and water as well as ionic components dissolved/bound in complexes as liquid impurities. After upgrading at 150 °C (Fig. 5) just some residues of DMF and the complexes may remain. With the control experiment at an imprint temperature as low as 75 °C (Fig. 6) the liquid impurities remain unchanged; admittedly, water-induced degradation products ($PbBr_2$, MABr) have to be expected due to the long imprint time (1 h). In contrast, pristine layers prepared at $T_{SB2} = 125$ °C should contain a reduced amount of liquid impurities, some DMF and potentially some water as well as some ionic impurities dissolved/ bound in complexes. After an upgrading at 150 °C (Fig. 5) in particular the water content should be reduced; furthermore, PbO (from decomposition/dehydration of $Pb(OH)_2$) has to be expected. In fact, XRD measurements suggest the presence of PbO (see Fig. S-A4).

The implications of any excess material present in the layers become evident after unloading and, in particular, after vacuum exposition. With hot loading, the samples are still on the hotplate after pressure release, however, the tight contact to the stamp is lost and any gaseous components will evaporate. Subsequent vacuum exposition will further remove components that are gaseous at the respective pressure. With that in mind the experimental results can be understood in parts.

We suggest that the depleted holes as well as the grainy and porous regions result from the evaporation of excess material still present in the layer after upgrading. The larger hole size and the wider porous regions observed with the lower soft-bake temperature (Fig. 5) correlate well with the higher amount of excess material contained in the pristine layers, in particular with the control experiment (Fig. 6, imprint at 75 °C). We conclude that the 'seas' of Fig. 6a) that 'empty' upon vacuum exposition contain a substantial amount of excess material; though liquid in pure form the ionic mixture/complexes show a certain stability and just evaporate after some time of vacuum exposure, here several days. Whereas EDX is less suited to prove the reduction of the organic compounds it clearly shows the decrease in the bromine content with vacuum exposition (see Tab. S-B6); this may indicate that the surplus of Br in the layers mainly consists of dissociated MABr dissolved/bound in complexes rather than solid MABr (low vapour pressure). The solid residue remaining in some of the holes is primarily $PbBr_2$ (Fig. S-B3) with some admixture, as e.g. PbO (Fig. S-A4).

3.2.3 Re- and post-crystallization

Our pristine layers contain different amounts of excess material, which, in parts, can also be considered as precursors for the perovskite envisaged. Therefore, we differentiate between recrystallization (here: grain re-formation/nucleation for stress relaxation [51, 54] plus subsequent grain growth on the cost of other grains) and a process we call 'post-crystallization'. With post-crystallization additional perovskite is formed locally from the excess material. Recrystallization and post-crystallization occur in parallel at our imprint temperature of 150 °C.

During recrystallization the grains grow and excess material is expelled from the growing grains. Figure 5c, d) clearly shows its aggregation at grain boundaries and grain boundary junctions by the porous regions and holes observed after vacuum exposition. However, ongoing grain growth should then increase the amount of excess material near the grain boundaries, which is not the case (Fig. 5e, f). In contrast, the porous regions clearly decrease in width, while the volume occupied by the holes remains largely constant (Table 2).

Introducing post-crystallization helps to understand this last feature of the experiments. We suggest that post-crystallization occurs in regions where a large amount of excess material is agglomerated, thus reducing the amount of excess material remaining locally. Ongoing recrystallization shifts further excess material towards the grain boundaries replenishing the supply there. We suppose that post-crystallization occurs near the periphery of the purified perovskite grains, at the transition to the porous region observed later (which decreases in size with increasing imprint time).

If post-crystallization is to occur, the peripheral regions of the growing grains have to contain compounds suitable for further perovskite formation. As the effect is much more distinct with the lower soft-bake temperature we assume that the 2 min at $T_{SB1} = 75$ °C were not sufficient for a complete consumption of the precursor. Then, the pristine layers prepared at $T_{SB1} = 75$ °C will also contain a certain amount of precursor remaining, MABr and $Pb(AcO)_2$; at $T_{SB2} = 125$ °C precursor rests are only minor (see also Fig. S-A2);—according to Table 1 the (solid) precursor components are stable enough to survive the treatment at 150 °C. $PbBr_2$ (and MABr) from (water-induced) degradation together with ionic components dissociated/bound in complexes are further potential candidates to contribute to post-crystallization during the recrystallization step. Lead from $Pb(OH)_2$ and dehydrated to PbO is most likely lost for post-crystallization (though sometimes claimed to be suited for perovskite preparation [55]).

From the decreasing porous or grainy regions with time we conclude that post-crystallization is prominent when a layer that was prepared at $T_{SB1} = 75$ °C is upgraded by an imprint at 150 °C (Fig. 5c, e). With a layer prepared at $T_{SB2} = 125$ °C (Fig. 5d, f) post-crystallization is less prominent. In contrast, when a layer prepared at $T_{SB1} = 75$ °C is imprinted at a temperature as low as 75 °C (control experiment) post-crystallization is negligible; accordingly, we observed wide porous or grainy regions even after a 1-h imprint under such conditions (Fig. 6c).

3.2.4 Concept

Now, based on the ideas developed to understand the specific features observed in the experiments a concept for the physical processes involved in the imprint-induced upgrading of perovskite layers can be developed. We start with the experiment according to Fig. 6, the control experiment, i. e. a layer soft-baked at 75 °C and imprinted at this temperature as well. The main steps are sketched in Fig. 7.

The initial situation (1) features a sample with an imperfect perovskite layer, containing a high amount of impurities, our excess material. From the discussion above we know that at a soft-bake temperature of 75 °C the layer will contain (in addition to the perovskite and precursor rests) a high amount of liquid excess material, namely AcOH, MAAc, DMF, water and ionic components in complexes. During imprint (2/3), when temperature and pressure are applied, recrystallization occurs (not considered in the sketch). Though the size of the continuous grains increases only slightly when imprinted at 75 °C (by a factor of 3.5), impurities are expelled out of the growing crystals [48]. During this process the stamp acts as a cover; it prevents the escape of any material and it directs recrystallization to the lateral direction. The impurities are transported towards the grain boundaries (indicated in (2) by the gradient of colour and the black arrows) resulting in an increase in the respective concentration. We expect that the ionic components form a 'quasi-liquid' mixture of complexes near the grain boundaries, where the concentration of impurities is highest.

In addition, the concentration of water plays a critical role here; as already addressed it represents a solvent for methylammonium-based perovskites [25] as it dramatically reduces the coordination strength between the ionic components involved [53]. Excess water becomes expelled from the grains (—hydrated crystals are not stable at 75 °C [35]) where, from some position on, the critical amount of water (3 molecules per perovskite unit [25], see text in context with Eq. 3) is exceeded. Accordingly, we assume a local dissolution of $MAPbBr_3$ by water (in addition to DMF) near the grain boundaries that contributes to the quasi-liquid mixture.

This quasi-liquid mixture forms a network of channels along the grain boundaries. Forced by grain growth, this (almost incompressible) liquid is transported along the grain boundaries (3a) to assemble at grain boundary junctions (3b); top views of the respective situations are shown at the bottom, left column, and at the top, right column of

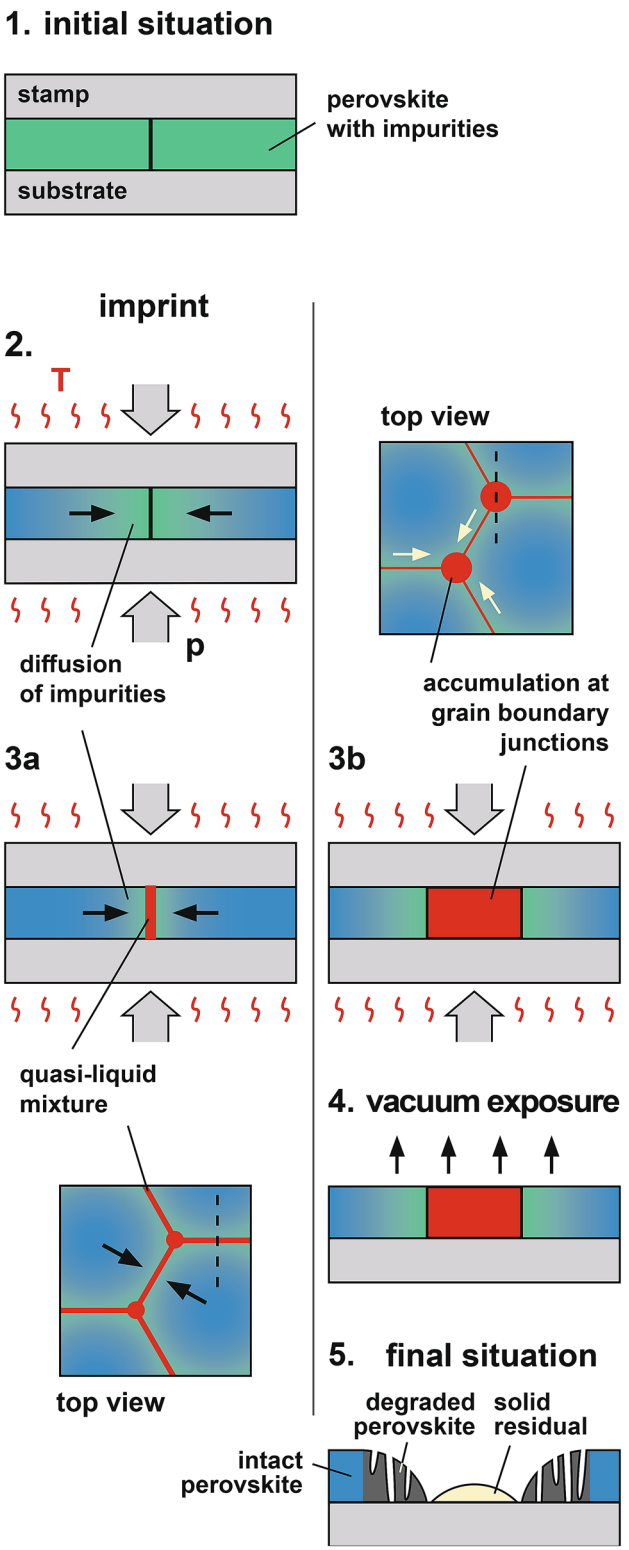

Fig. 7 Concept of physical processes involved in upgrading a polycrystalline perovskite layer via thermal imprint with a flat stamp, taking the example of a pristine layer prepared at a soft-bake temperature of 75 °C. ('Impurities' stands for the multiple excess materials contained in the layer, see text). Left: Cross section through grain boundary (see top view at the bottom). Right: Cross section through grain boundary junction (see top view at the top)

Fig. 7, indicating the transport of the impurities (arrows) and the respective cross section for 3a/b (dashed). At the grain boundary junctions, the liquid mixture accumulates (red spots), where the 'seas' of Fig. 6a) develop in the first instance (3b). To the end, the excess material and the dissolved perovskite are concentrated there locally, the surrounding grains still containing some impurities/excess material close to their boundaries.

During a subsequent vacuum exposition of the sample after stamp removal (4) all components that are volatile at the pressure used are vapourized. This results in the final situation (5) with holes, where only accumulated components remain that are relatively stable under vacuum, here a mixture of $PbBr_2$, MABr (from local water-induced degradation, Eq. 3) and PbO as well as precursor rests. Swift evaporation of gaseous components during vacuum exposition at room temperature (reduced mobility) from this multi-component mixture may be the reason why the solid residual does not feature any apparent sign of crystallinity. The vapourized impurities from the periphery of the perovskite grains result in the typical porous rim around the holes;—the surface curvature may indicate the concentration gradient of the impurities inside the grains, in good accordance with Fig. 6c.

This concept derived for worst case conditions ($T_i = T_{SB1} = 75$ °C) can easily be transferred to the situation with an imprint at 150 °C. The main difference then is that post-crystallization comes into play. The situation with $T_{SB2} = 125$ °C is most simple. Then water is not an issue and local dissolution of the perovskite is not likely; similarly, AcOH and MAAc drop out leaving just DMF as the liquid component, together with ionic complexes. Nonetheless, during recrystallization an accumulation of excess material near grain boundaries similarly occurs. Besides PbO (from decomposed $Pb(OH)_2$), the solid remaining in some holes most likely is just $PbBr_2$. (A similar finding is reported by Wang [50] upon annealing of $MaPbI_3$ layers resulting from solvent-induced complex formation.) We expect a limited effect of post-crystallization only as almost no precursor should have remained after soft-bake.

When a layer soft-baked at $T_{SB1} = 75$ °C is exposed to 150 °C under hot loading conditions some of the water, DMF, AcOH and Br-complexes contained may evaporate within the 20–30 s before the pressure is applied; however, a substantial amount of these liquid components will remain during recrystallisation. (The remaining water may still be effective for localized perovskite dissolution at grain boundaries; however, its contribution to the liquid mixture is reduced compared to the control experiment at 75 °C.) Post-crystallization should be distinct during recrystallization as the precursor has not been completely depleted during soft-bake. Besides MABr (e.g. from water-induced degradation) and PbO, $PbBr_2$ should be the main residual between the grains after cool-down and vacuum exposition.

Any (partly filled) holes and porous regions indicate that the perovskite layers still contained excess material, which evaporated in parts during vacuum exposition. Grains without holes should be largely free from impurities. Therefore, SEM analysis, in particular after vacuum exposition, is a simple means to assess the quality of a recrystallized perovskite layer in terms of the presence of excess material that may affect the electrical and optical properties of perovskite-based devices in the long term. In this context Fig. 5 also documents that, albeit not significant for grain growth during re-crystallisation, an increased imprint time results, after all, in crystal grains of a higher grade of purity as the porous regions decrease.

3.2.5 Perovskite degradation during imprint

Though we upgrade the perovskite layers at 150 °C, a temperature where the material is prone to decomposition, degradation (though present sparsely, see Fig. S-A4) has not yet been discussed in detail. This is now concluded, for the hot loading experiments according to Fig. 5.

With hot loading, the imprint stack is not loaded before the system is heated up completely. As mentioned, placing the sachet with the imprint stack correctly on to the preheated hotplate and applying the full pressure takes about 20–30 s. During this time the sample is just annealed, and this happens under the ambient atmosphere in the sachet. This annealing already leads to crystal growth, however, simultaneously some thermal decomposition of the material may occur, where, in addition, water (ambient humidity in the sachet as well as residual water from the trihydrate) may attack the perovskite (see Eq. 2). Experiments where the sachet was loaded to the hotplate and annealed (without any pressure application) for time spans of 10 s to 30 s verified that holes develop, preferably at grain boundary junctions, with both soft-bake temperatures as well. However, their size is in the range of 200 nm–300 nm, only, taking up ≈ 1.5% of the overall area. Holes of that size are easily closed upon pressure application, they are not an issue with upgrading. This is different with potential degradation products. Volatile decomposition products are held within the sachet by the Al-wrap; nevertheless, they diffuse around, away from their point of origin; as a consequence, they may be lost for any subsequent local re-formation of the perovskite. The solid decomposition products stay in the layer. As impurities they may affect recrystallization, reducing the grain size obtainable [54]. To minimize degradation, we held this time span without pressure limited by swift loading enabled by the use of the sachet.

As soon as the pressure is applied the situation changes markedly; due to the tight contact to the stamp the perovskite layer then is largely shielded from atmosphere. Thermal degradation may occur but now the decomposition products stay close to their point of origin and may still take part in the recrystallization process. Stamp and substrate do not only restrict grain growth to the respective gap, they also act similar to an encapsulation of the perovskite, as e.g. shown with solar cells [56]; – all primary degradation reactions are reversible as long as the components involved stay in place so that the local stoichiometry remains unchanged [26], whereby gaseous components may be trapped in the crystal [57]. With conventional processing (anneal without cover) this is usually not the case due to the volatile character [24, 58] of MMA and HBr, see Eq. 2. This emphasizes the special role of the protective stamp with our experiments;—in the literature referring to Cs-based perovskites, where all degradation products are non-volatile, reversible degradation reactions in fact are reported [59, 60], thus supporting our arguments. The consequence is that the amount of decomposition products should not increase substantially under tight stamp contact, i. e. during imprint-induced recrystallization.

At the end of the hot loading process the pressure is released at processing temperature. During the cool-down to room temperature of about 2 min again some degradation is possible, similar to that just before pressure application. However, now the grains are larger and the overall length of the grain boundaries has decreased (grain boundaries are most susceptible to degradation), so that the risk of degradation is reduced compared to the initial phase of hot loading. Again, any gaseous decomposition products would escape the layer when the stamp pressure is removed, before unloading the sachet and before separating stamp and sample.

As the time susceptible to decomposition is short compared to the overall processing time during our hot loading experiments, we conclude that thermal degradation is not a main issue, due to the protective effect of the stamp. This protective effect is confirmed by EDX results (Tab. S-B8); the composition of the pristine layer does not change due to hot loading.

In particular, degradation cannot account for the holes observed; as already discussed we assume that the holes result from the partial evaporation of aggregated excess material. Despite the increased temperature the relative area occupied by holes with an imprint at 150 °C (≈5%) is smaller than with an imprint at 75 °C (≈9%). However, with hot loading degradation may somewhat contribute to the holes within the times and locations without tight stamp contact. Nonetheless, the dominating effect of the stamp during the upgrading step is to protect the layer against degradation and to restrict the grain growth to the lateral direction, so that largely continuous and flat perovskite layers with grains spanning the whole gap between stamp and substrate are formed.

3.2.6 Processing-related aspects

When upgrading perovskite layers by thermal imprint the uniformity obtained is limited. Most often, some millimetres-sized regions of dense grains and less dense grains are found nearby [18]. Accordingly, the SEM micrographs documenting the hot loading experiments (Figs. 5, 6) were chosen to show a 'typical' situation, somewhere in between dense and rather loosely arranged grains. The reason for this local nonuniformity is still under discussion. A local variation of the quality of the pristine layer with respect to the side-products does not apply, as layers that simply were annealed feature a better uniformity.

We assume that the reason is imprint-related. With plate-to-plate imprint systems as the one used here [43] it is well known that a locally varying gap between the stamp surface and the perovskite surface may exist for some time, due to some inevitable waviness of all surfaces involved, the stamp, the substrate and the press plates as well [61]. In addition, individual single crystalline grains in the pristine layer may act as temporary spacers [62] between stamp and substrate; such local temporary gaps during the initial phase of imprint come along with a somewhat inhomogeneous pressure distribution. When a tight contact between the surface of the sample and the stamp is not ensured at high temperature, degradation may affect the upgrading result. With such a temporary local gap degradation without perovskite re-formation may occur and may be one of the reasons for the less dense regions observed.

Furthermore, all components contained in the layer after soft-bake are held in the layer under pressure during the whole upgrading process and cannot escape. In particular, liquid excess material stays liquid. (As for water, the boiling point is shifted to >300 °C at 100 bar). As a consequence, the 'quasi-liquid' mixture introduced with the control experiment would be similarly effective not only to transport excess material towards grain boundary junctions but also into regions of temporary gaps and thus reduced pressure, so that an accumulation of impurities in such regions would be likely. (As long as the gap exists and the full imprint pressure is not active liquid components may evaporate meanwhile, until the gap closes with ongoing imprint.) Such an accumulation of excess material in local regions where a temporary gap existed may also explain the less dense regions. Further investigations will address this issue in detail.

3.3 Planar hot pressing

Now, as detailed analysis of the hot loading experiments has established a conceptual understanding of the underlying physical basics, the standard process used for upgrading perovskite layers is revisited, planar hot pressing (PHP). In contrast to hot loading, the layer is under imprint pressure throughout the whole PHP process, from heat-up to cool-down (compare Fig. 2). The imprint at 150 °C (100 bar) was performed for 5 min, a typical imprint time. The results of Fig. 5 do not indicate that an increased time would improve recrystallization; moreover, crystal growth as a temperature-activated process driven by energy minimization will start before the actual imprint temperature is reached.

Figure 8 presents typical PHP results. The mean size of connected crystalline regions is somewhat larger with the higher soft-bake temperature, about 1.3 µm with 75 °C and about 2.2 µm with 125 °C. It indicates a remarkable grain growth, in particular with the samples prepared at the lower soft-bake temperature;—the respective pristine layer had grains of about 111 nm (75 °C) and 350 nm (125 °C), only.

Generally, PHP should reduce the impact of global degradation compared to hot loading. With the exception of unintentional temporary gaps at the beginning (see Sect. 3.2.6) the perovskite is under full pressure during the whole process. Any degradation product built is held in place and some equilibrium may establish between perovskite decomposition and re-formation. Thus, global degradation of the perovskite layer due to temperature and humidity should be negligible, with the sachet used and without it. This is in accord with XRD measurements (see Fig. S-A7).

However, local dissolution by residual water and DMF near the grain boundaries during recrystallization is an issue. As the pristine layer prepared at $T_{SB1} = 75$ °C should contain, in addition, liquid AcOH and potentially MAAc, the network of channels is effective during the whole PHP process to redistribute excess material between the grains;—water from thermal decomposition of $Pb(OH)_2$ into PbO during PHP may contribute. Due to the long overall recrystallization time during PHP (about 20 min due to heat-up and

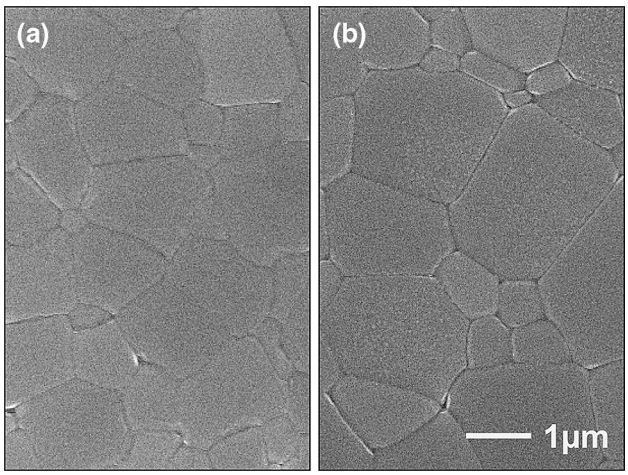

Fig. 8 Planar hot pressing (PHP) result with $MAPbBr_3$, **a** $T_{SB1} = 75$ °C and **b** $T_{SB2} = 125$ °C. (Imprint: pressure 100 bar, temperature 150 °C, time 5 min)

cool-down adding in part to the imprint time) all the impurities had enough time to accumulate at grain boundaries and at grain boundary junctions, maximizing recrystallization and post-crystallization.

Definitely, porous regions are not typical with the PHP process, which indicates a high purity of the perovskite layer with continuous grains (see Fig. S-B4). Similar to hot loading, any residues should consist of $PbBr_2$ with some MABr (from local water-induced degradation); due to efficient post-crystallization at 150 °C any precursor rests are not expected.

Figure 8 documents that even with pristine layers prepared under different conditions a similar upgrade of the perovskite by planar hot pressing was possible, resulting in largely continuous grains of high purity and high flatness (see Fig. S-B4). The atomic composition in regions with dense grains is near to 3:1 (see Tab. S-B7), similar as with the pristine layers and after hot loading. Furthermore, PHP also demonstrates the protective effect of the stamp (Tab. S-B8), any material present in the pristine layer stays there during PHP. This implies that products that are gaseous at the imprint temperature of 150 °C cannot escape, thus preserving the integrity of the layer. It can be anticipated that a precursor other than the acetate, without any remaining rest (e.g. $PbBr_2$ as the Pb-precursor) will even improve the connectivity of the grains after a PHP-upgrade. Future research will address this issue.

3.4 Consequences for application

Our intention was to advance the preparation of methylammonium-based perovskites with respect to scalable and reproducible industrial processing. A number of direct consequences for application can be drawn from the results obtained.

The investigation has demonstrated that thermal nanoimprint is a highly promising candidate for upgrading polycrystalline perovskite layers. Protected by the stamp, micron-sized grains are achieved within short times (minutes) as temperatures higher than conventional annealing temperatures can be applied without degrading the layers. Short upgrading times foster throughput and may facilitate roller-based processing;—beyond the plate-to-plate technique used here, thermal imprint may also be operated as a roll-to-plate or a roll-to-roll process where heat-up times are not an issue. Moreover, besides recrystallization also post-crystallisation is effective to achieve a complete conversion of potential precursor components into the perovskite. This may be of impact in combination with alternative large-area coating techniques (e.g. slot die coating), to skip a separate annealing step. In addition, processing under ambient atmosphere should be possible due to the effective shielding by the stamp during the PHP process. The upgrading of layers by simple post-processing is an important step to decouple the layer quality required for operational devices from the initial layer deposition.

A further issue is the control of the layer quality, especially when measurement techniques like X-ray diffraction or Raman spectroscopy are not available or too sophisticated, as e.g. with large-area manufacturing. We have shown that the change in the morphology during vacuum exposition indicates non-perovskite constituents in the layer. The key is that some of the typical excess materials still present in the pristine layer are volatile under vacuum, which becomes evident in the formation of partly filled holes and porous regions. Thus, the inspection of a recrystallized layer after exposition to a rough vacuum represents a simple test of the overall quality of the perovskite layer requiring only moderate efforts on the equipment. When the vacuum-induced defects are in the micrometre range the SEM inspection used here may be replaced by conventional optical inspection techniques, as e.g. reflection. Of course, a further qualification of such optical testing techniques is necessary, but they have a high potential for the inspection of large-area processes which will be required for manufacturing.

Furthermore, the use of acetates as cost-efficient lead sources for perovskites turned out to be critical. Even when the formulation of the solution with the precursors matches the exact stoichiometry residuals from the acetate group may remain in the layer. The acetate itself may be removed by an adequate soft-bake temperature, but due to the high polarity the risk of a formation of side-products or complexes remaining in the layer is high; the layers are prone for impurities. As PbO is detected after upgrading, the formation of $Pb(OH)_2$ (or $PbO{\cdot}H_2O$) from dissociated $Pb(AcO)_2$ is probable; this will reduce the amount of lead available for perovskite formation and limit the conversion of the precursors into $MAPbBr_3$. (Admittedly, without excess Br in the layers (as with our experiments) some of the adverse effects observed here may become mitigated; however, they enabled us to develop a physical understanding of the mechanisms involved in imprint-induced upgrading.) Definitely, in case of the trihydrate a soft-bake temperature beyond 100 °C is advised to reduce the water content. Our impression is that the use of acetates as the lead precursor for perovskites is a compromise between cost and layer quality. A promising route with a reduced lead acetate content has been demonstrated for $MAPbI_3$ [63].

4 Summary and conclusions

We investigated methylammonium-based perovskites with $Pb(AcO)_2$-trihydrate as the lead precursor, typically resulting in polycrystalline layers with a relatively high amount of impurities. Our investigation has demonstrated that thermal

imprint is well suited for upgrading these polycrystalline layers. This is due to the stamp that enables recrystallization at temperatures much higher than conventional annealing temperatures. The stamp shields the layer from atmosphere during the whole recrystallization in a PHP process due to the pressure applied. All components present in the layer stay there and do not evaporate, so that degradation is negligible and an efficient conversion of the precursor into perovskite is ensured by post-crystallization, if appropriate. Yet, with a pristine layer containing a high amount of excess material continuous grains of some micron size were obtained after planar hot pressing.

A technique named hot loading was applied to investigate the temporal evolution of the upgrading process at 150 °C. It turned out that recrystallization is a fast process; already after less than 60 s micron-sized grains were obtained. During recrystallization the stamp directs grain growth to the lateral direction, resulting in highly flat polycrystalline layers. Any excess, non-perovskite material within the layer agglomerates near grain boundaries and grain boundary junctions. Experiments with pristine layers containing different amounts of side-products showed that excess material is re-arranged between the growing grains and that post-crystallization occurs. This is in particular prominent with a layer prepared at a low soft-bake temperature where precursor conversion was incomplete.

A concept was developed to understand the physical processes involved in upgrading. Upon recrystallization the excess material still present in the layer that is expelled from the grains is efficiently transported as a quasi-liquid mixture of ionic/polar components along a network of channels at grain boundaries to accumulate locally. Subsequent vacuum exposition was used to document the existence of such excess material by partial evaporation. Such a procedure has a high potential for an optical control of the overall quality of an upgraded perovskite layer in the future.

In total, thermal imprint represents an effective means to improve perovskite layers by post-processing, providing a simple physical alternative to the numerous chemical approaches reported so far. In particular planar hot pressing (PHP) is suitable to decouple the preparation of high-quality perovskite layers with large grains from the initial layer deposition, a vital step towards reliable industrial processing of devices in future. Upgrading non-perfect perovskite layers by imprint could be a tool to manufacture high-quality perovskite layers over large areas at low cost.

Supplementary Information The online version contains supplementary material available at. https://doi.org/10.1007/s00339-021-04366-3.

Acknowledgement Financial support from the Deutsche Forschungsgemeinschaft (DFG) is highly acknowledged (contracts RI 1551/9-1 and SCHE 580/23-1). The authors also appreciate support with TGA characterization by A. Helfer / U. Scherf, Chair for Macromolecular Chemistry, University Wuppertal and T. Haeger, Chair for Electronic Devices, University Wuppertal, for preparation of some of the layers.

Funding Open Access funding enabled and organized by Projekt DEAL.

Compliance with ethical standards

Conflict of interest The Authors declare that there is no conflict of interest.

References

1. A. R. B. Mohd Yusoff, P. Gao, M. K. Nazeeruddin, Coord. Chem. Rev. **373**, 258 (2018).
2. S. Tao, I. Schmidt, G. Brocks, J. Jiang, I. Tranca, K. Meerholz, S. Olthof, Nat. Commun. **10**, 2560 (2019)
3. M. Jung, S.-G. Ji, G. Kim, S.I. Seok, Chem. Soc. Rev. **48**, 2011 (2019)
4. J. Zhang, W. Zhang, H.-M. Cheng, S.R.P. Silva, Mater. Today **39**, 66 (2020)
5. Y. Tian, C. Zhou, M. Worku, X. Wang, Y. Ling, H. Gao, Y. Zhou, Y. Miao, J. Guan, B. Ma, Adv. Mater. **30**, 1707093 (2018)
6. N. Pourdavoud, A. Mayer, M. Buchmüller, K. Brinkmann, T. Häger, T. Hu, R. Heiderhoff, I. Shutsko, P. Görrn, Y. Chen, H.-C. Scheer, T. Riedl, Adv. Mater. Technol. **3**, 1700253 (2018)
7. M. Ahmadi, T. Wu, B. Hu, Adv. Mater. **29**, 1605242 (2017)
8. R. Patidar, D. Burkitt, K. Hooper, D. Richards, T. Watson, Mater. Today Commun. **22**, 100808 (2020)
9. Q. Hu, L. Zhao, J. Wu, K. Gao, D. Luo, Y. Jiang, Z. Zhang, C. Zhu, E. Schaible, A. Hexemer, C. Wang, Y. Liu, W. Zhang, M. Grätzel, F. Liu, T.P. Russell, R. Zhu, Q. Gong, Nat. Commun. **8**, 15688 (2017)
10. F. Mathies, H. Eggers, B.S. Richards, G. Hernandez-Sosa, U. Lemmer, U.W. Paetzold, A.C.S. Appl, Energy Mater. **1**, 1834 (2018)
11. M. Xiao, F. Huang, W. Huang, Y. Dkhissi, Y. Zhu, J. Etheridge, A. Gray-Weale, U. Bach, Y.-B. Cheng, L. Spiccia, Angew. Chem. Int. Ed. **53**, 9898 (2014)
12. N.J. Jeon, J.H. Noh, Y.C. Kim, W.S. Yang, S. Ryu, S.I. Seok, Nat. Mater. **13**, 897 (2014)
13. S. Ternes, T. Börnhorst, J.A. Schwenzer, I.M. Hossain, T. Abzieher, W. Mehlmann, U. Lemmer, P. Scharfer, W. Schabel, B.S. Richards, U.W. Paetzold, Adv. Energy Mater. **9**, 1901581 (2019)
14. T. Seewald, E.R. Schütz, C. Ebenhoch, L. Schmidt-Mende, J. Phys. Energy **2**, 021001 (2020)
15. N. Pourdavoud, S. Wang, A. Mayer, T. Hu, Y. Chen, A. Marianovich, W. Kowalsky, R. Heiderhoff, H.-C. Scheer, T. Riedl, Adv. Mater. **29**, 1605003 (2017)

16. N. Pourdavoud, T. Haeger, A. Mayer, P.J. Cegielski, A.L. Giesecke, R. Heiderhoff, S. Olthof, S. Zaefferer, I. Shutsko, A. Henkel, D. Becker-Koch, M. Stein, M. Cehovski, O. Charfi, H. Johannes, D. Rogalla, M.C. Lemme, M. Koch, Y. Vaynzof, K. Meerholz, W. Kowalsky, H. Scheer, P. Görrn, T. Riedl, Adv. Mater. **31**, 1903717 (2019)
17. H. Cho, J.S. Kim, Y.-H. Kim, T.-W. Lee, J. Inform, Display **19**, 53 (2018)
18. A. Mayer, M. Buchmüller, S. Wang, C. Steinberg, M. Papenheim, H.-C. Scheer, N. Pourdavoud, T. Haeger, T. Riedl, J. Vac. Sci. Technol. B **35**, 06G803 (2017)
19. C. Aranda, C. Cristobal, L. Shooshtari, C. Li, S. Huettner, A. Guerrero, Sustain. Energy Fuels **1**, 540 (2017)
20. N. Giesbrecht, J. Schlipf, L. Oesinghaus, A. Binek, T. Bein, P. Müller-Buschbaum, P. Docampo, ACS Energy Lett. **1**, 150 (2016)
21. C. Li, Q. Guo, Z. Wang, Y. Bai, L. Liu, F. Wang, E. Zhou, T. Hayat, A. Alsaedi, Z. Tan, A.C.S. Appl, Mater. Interf. **9**, 41937 (2017)
22. X. Tang, M. Brandl, B. May, I. Levchuk, Y. Hou, M. Richter, H. Chen, S. Chen, S. Kahmann, A. Osvet, F. Maier, H.-P. Steinrück, R. Hock, G.J. Matt, C.J. Brabec, J. Mater. Chem. A **4**, 15896 (2016)
23. J.I.J. Choi, M.E. Khan, Z. Hawash, K.J. Kim, H. Lee, L.K. Ono, Y. Qi, Y.-H. Kim, J.Y. Park, J. Mater. Chem. A **7**, 20760 (2019)
24. J.M. Frost, K.T. Butler, F. Brivio, C.H. Hendon, M. van Schilfgaarde, A. Walsh, Nano Lett. **14**, 2584 (2014)
25. A.M.A. Leguy, Y. Hu, M. Campoy-Quiles, M.I. Alonso, O.J. Weber, P. Azarhoosh, M. van Schilfgaarde, M.T. Weller, T. Bein, J. Nelson, P. Docampo, P.R.F. Barnes, Chem. Mater. **27**, 3397 (2015)
26. E.J. Juarez-Perez, L.K. Ono, M. Maeda, Y. Jiang, Z. Hawash, Y. Qi, J. Mater. Chem. A **6**, 9604 (2018)
27. X.B. Cao, C.L. Li, L.L. Zhi, Y.H. Li, X. Cui, Y.W. Yao, L.J. Ci, J.Q. Wei, J. Mater. Chem. A **5**, 8416 (2017)
28. I.L. Ivanov, M.O. Mazurin, D.S. Tsvetkov, D.A. Malyshkin, V.V. Sereda, AYu. Zuev, Thermochim. Acta **674**, 58 (2019)
29. Lead(II) Acetate.3aq v.p. (Chem-Lab N.V., Zedelgem, Belgium, 2018).
30. Methylamine Acetate (TCI Europe N.V., Zwijndrecht, Belgium, 2019).
31. Y. Xia, C. Ran, Y. Chen, Q. Li, N. Jiang, C. Li, Y. Pan, T. Li, J. Wang, W. Huang, J. Mater. Chem. A **5**, 3193 (2017)
32. H. Schoen, *Handbook of Purified Gases* (Springer, Berlin, Heidelberg, 2015).
33. K. Aim, Fluid Phase Equilib. **2**, 119 (1978)
34. M.A. Mohamed, S.A. Halawy, M.M. Ebrahim, Thermochim. Acta **236**, 249 (1994)
35. F.J. Martínez-Casado, M. Ramos-Riesco, J.A. Rodríguez-Cheda, F. Cucinotta, E. Matesanz, I. Miletto, E. Gianotti, L. Marchese, Z. Matěj, Inorg. Chem. **55**, 8576 (2016)
36. P. Patnaik, *Handbook of Inorganic Chemicals* (McGraw-Hill, New York, 2003).
37. D.R. Lide (ed.), *CRC Handbook of Chemistry and Physics*, 84th edn. (CRC Press LCC, Boca Raton, 2003)
38. Methylammoium Bromide (Sigma-Aldrich Chemie GmbH, Taufkirchen, Germany, 2019).
39. R.H. Perry, D.W. Green, J.O. Maloney (eds.), *Perry's Chemical Engineers' Handbook*, 7th edn. (McGraw-Hill, New York, 1997)
40. L. Dimesso, M. Dimamay, M. Hamburger, W. Jaegermann, Chem. Mater. **26**, 6762 (2014)
41. M. Kulbak, S. Gupta, N. Kedem, I. Levine, T. Bendikov, G. Hodes, D. Cahen, J. Phys. Chem. Lett. **7**, 167 (2016)
42. A. Mayer, S. Moellenbeck, K. Dhima, S. Wang, and H.-C. Scheer, J. Vac. Sci. Technol. B **29**, 06FC13 (2011).
43. A. Mayer, K. Dhima, S. Möllenbeck, S. Wang, H.-C. Scheer, Proc. SPIE **8352**, 83520N (2012)
44. C. Steinberg, K. Dhima, D. Blenskens, A. Mayer, S. Wang, M. Papenheim, H.-C. Scheer, J. Zajadacz, K. Zimmer, Microelect. Eng. **123**, 4 (2014)
45. A. Mayer, K. Dhima, S. Wang, C. Steinberg, M. Papenheim, H.-C. Scheer, Appl. Phys. A **121**, 405 (2015)
46. C. Wang, B.R. Ecker, H. Wei, J. Huang, Y. Gao, J. Phys. Chem. C **122**, 3513 (2018)
47. I. Deretzis, A. Alberti, G. Pellegrino, E. Smecca, F. Giannazzo, N. Sakai, T. Miyasaka, A. La Magna, Appl. Phys. Lett. **106**, 131904 (2015)
48. D. A. Porter, K. E. Easterling, and M. Y. Sherif, *Phase Transformations in Metals and Alloys*, 3rd ed. (CRC Press, Taylor & Francis Group, Boca Raton, 2009).
49. J.-W. Lee, S.-H. Bae, Y.-T. Hsieh, N. De Marco, M. Wang, P. Sun, Y. Yang, Chemistry **3**, 290 (2017)
50. S. Wang, Z. Ma, B. Liu, W. Wu, Y. Zhu, R. Ma, C. Wang, Sol. RRL **2**, 1800034 (2018)
51. D. Raabe, *In Physical Metallurgy*, 5th edn. (Elsevier, Amsterdam, 2014), pp. 2291–2397
52. F.A. Roghabadi, M. Alidaei, S.M. Mousavi, T. Ashjari, A.S. Tehrani, V. Ahmadi, S.M. Sadrameli, J. Mater. Chem. A **7**, 5898 (2019)
53. Y. Zhang, F. Huang, Q. Mi, Chem. Lett. **45**, 1030 (2016)
54. E.J. Mittemeijer, *Fundamentals of Materials Science* (Springer, Berlin, Heidelberg, 2011).
55. J. Huang, K. Jiang, X. Cui, Q. Zhang, M. Gao, M. Su, L. Yang, Y. Song, Sci. Rep. **5**, 15889 (2015)
56. K.O. Brinkmann, J. Zhao, N. Pourdavoud, T. Becker, T. Hu, S. Olthof, K. Meerholz, L. Hoffmann, T. Gahlmann, R. Heiderhoff, M.F. Oszajca, N.A. Luechinger, D. Rogalla, Y. Chen, B. Cheng, T. Riedl, Nat. Commun. **8**, 13938 (2017)
57. F.A. Roghabadi, V. Ahmadi, K.O. Aghmiuni, J. Phys. Chem. C **121**, 13532 (2017)
58. J. Yang, B.D. Siempelkamp, D. Liu, T.L. Kelly, ACS Nano **9**, 1955 (2015)
59. D. Di Girolamo, M.I. Dar, D. Dini, L. Gontrani, R. Caminiti, A. Mattoni, M. Graetzel, S. Meloni, J. Mater. Chem. A **7**, 12292 (2019)
60. M. Liu, J. Zhao, Z. Luo, Z. Sun, N. Pan, H. Ding, X. Wang, Chem. Mater. **30**, 5846 (2018)
61. M. Papenheim, *Flexible Komposit-Stempel für das Nanoimprint, PHD Thesis, University of Wuppertal* (Neopubli GmbH, Berlin, 2018).
62. A. Mayer, M. Papenheim, K. Dhima, S. Wang, C. Steinberg, H.-C. Scheer, F. Schröter, Microelect. Eng. **123**, 100 (2014)
63. K. O. Brinkmann, J. He, F. Schubert, J. Malerczyk, C. Kreusel, F. van gen Hassend, S. Weber, J. Song, J. Qu, and T. Riedl, ACS Appl. Mater. Interf. **11**, 40172 (2019).